ACS Macro Letters

Letter

pubs.acs.org/macroletters

Photochemical Design of Functional Fluorescent Single-Chain Nanoparticles

Johannes Willenbacher,[†,‡] Kilian N. R. Wuest,[†,‡] Jan O. Mueller,[†,‡] Michael Kaupp,[†,‡] Hans-Achim Wagenknecht,[§] and Christopher Barner-Kowollik*[,†,‡]

[†]Preparative Macromolecular Chemistry, Institut für Technische Chemie und Polymerchemie, Karlsruhe Institute of Technology (KIT), Engesserstr. 18, 76131 Karlsruhe, Germany

[‡]Institut für Biologische Grenzflächen, Karlsruhe Institute of Technology (KIT), Hermann-von-Helmholtz-Platz 1, 76344 Eggenstein-Leopoldshafen, Germany

[§]Institut für Organische Chemie, Karlsruhe Institute of Technology (KIT), Fritz-Haber-Weg 6, 76131 Karlsruhe, Germany

Supporting Information

ABSTRACT: We report the facile ambient temperature generation of size tunable and well-defined (pro)fluorescent single-chain nanoparticles (SCNPs) via the photoinduced nitrile imine intramolecular cross-ligation of linear precursor polymers, constituting a platform technology as novel imaging agents. A set of three linear precursor polymers ($M_n \approx 14000$ g mol^{-1}, $Đ \approx 1.25$) was synthesized via nitroxide-mediated statistical copolymerization of styrene and 4-(chloromethyl)styrene (CMS), followed by a postpolymerization modification of the resulting copolymer installing protected maleimide (PG-Mal) as well as tetrazole (Tet) moieties. The tetrazole content (% Tet) along the lateral polymer chains was varied between 12 and 24% in order to preselect not only the size of the corresponding SCNPs, but also their fluorescence and reactive properties. Finally, the applicability of the profluorescent SCNPs for fluorescence labeling was demonstrated utilizing residual surface expressed Tet moieties on the SCNPs surface in a reaction with maleimide functional polymeric microspheres. The (pro)fluorescent single-chain nanoparticles were in-depth characterized by ^{1}H NMR spectroscopy, dynamic light scattering (DLS), size exclusion chromatography (SEC), and atomic force microscopy (AFM), as well as UV/vis and fluorescence spectroscopy.

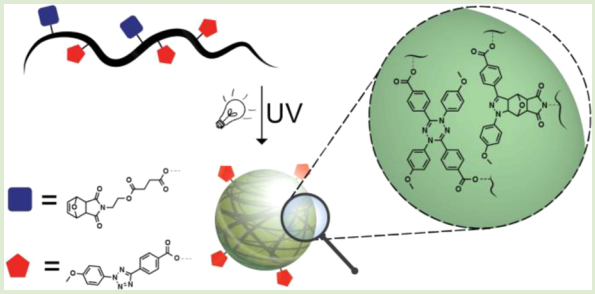

Single-chain nanoparticles (SCNPs) with diameters <20 nm, prepared via intramolecular cross-linking of single polymer chains, have attracted significant attention over the past few years due to their potential applications in catalysis, sensing, and drug delivery.[1−3] A further attractive area of their application is as cell transport and imaging agents, yet no viable, size tunable, and easy to prepare nanoparticle systems that display fluorescence and the corresponding excitation in the visible light region exist. Together with examples for polymer chains that have been folded at selective points along the backbone,[4−6] such single-chain architectures can be additionally regarded as potential synthetic mimics of proteins or peptides. The intramolecular cross-links in SCNPs can for instance be dynamic,[7,8] dynamic-covalent,[9,10] or covalent.[11−13] For covalently cross-linked SCNPs, to the best of our knowledge, only a small number of examples exists that take advantage of mild, phototriggered cross-linking approaches, and none present inherent fluorescent properties.[14−16] An example for fluorescent SCNPs was published by Oria et al. in 2010.[11] However, the fluorescence properties had to be imparted by employing a suitable cross-linker, and the fluorescence (391 and 410 nm), which has to be excited at λ_{exc} = 390 nm, is not suitable for biological applications.

In the present contribution, we introduce a powerful, intramolecular cross-linking chemistry for the fast preparation of inherently (pro)fluorescent SCNPs, which is based on the photoinduced nitrile imine mediated tetrazole-ene cycloaddition (NITEC).[17,18] UV-irradiation of tetrazole derivatives leads to the formation of nitrile imines, which are highly reactive 1,3-dipoles that are even capable of reacting with nonactivated alkene moieties.[19] The mild reaction conditions, the redundancy of a metal catalyst, and the fact that the resulting pyrazoline cycloadduct exhibits a broad fluorescence band in the visible spectral range makes the NITEC reaction a versatile tool not only for SCNP formation, but also for e.g., surface modifications,[20] polymer ligation,[21] protein functionalization,[22] and peptide modification.[23]

To make use of the NITEC approach for fabricating SCNPs, linear functional precursor polymers were synthesized via nitroxide mediated polymerization (NMP), a reversible-deactivation radical polymerization (RDRP) protocol, and a

Received: May 14, 2014
Accepted: May 29, 2014
Published: June 2, 2014

Scheme 1. Design Strategy for the Photochemical Preparation of Functional, (Pro)fluorescent Single-Chain Nanoparticles

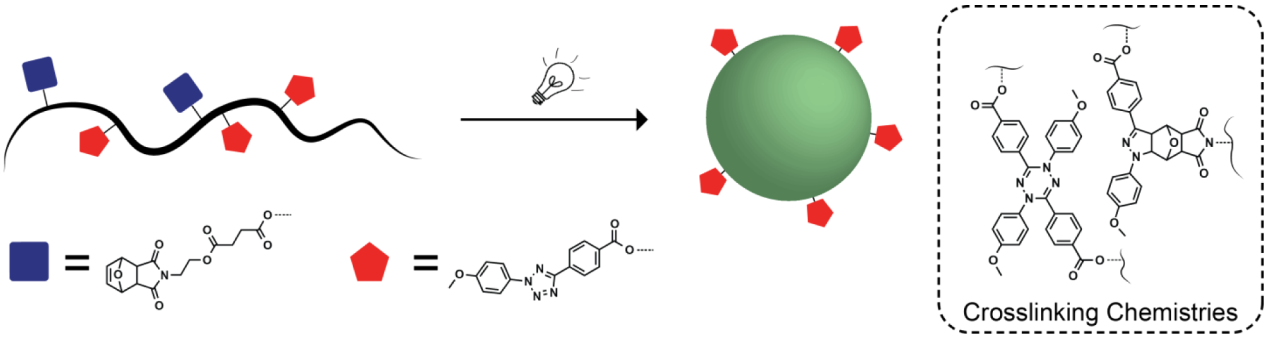

subsequent one-pot postpolymerization modification of the random copolymers with the NITEC components. The above-described strategy provides fine control over (*i*) the composition and (*ii*) chain length of the precursor polymer, concomitantly generating polymers with (*iii*) narrow molar-mass dispersities (*Đ*), three critical factors for the preparation of well-defined, functional SCNPs.

The size of single-chain nanoparticles is typically either controlled by varying the chain length of the precursor polymer or its degree of functionalization.[14] In the current approach we demonstrate how to control not only the size, but also the fluorescence properties of the SCNP by changing only the relative ratio of the NITEC components along the backbone of the precursor copolymer. The resulting (pro)fluorescent SCNPs are characterized by ^{1}H NMR spectroscopy, dynamic light scattering (DLS), size exclusion chromatography (SEC), and atomic force microscopy (AFM), as well as UV/vis and fluorescence spectroscopy. In addition, we show in an exemplary reaction with maleimide-functional microspheres that the residual, surface-expressed tetrazole moieties of the SCNPs can be utilized for further functionalization. The overall design strategy for the (pro)fluorescent SCNP generation is depicted in Scheme 1.

The functional linear precursor polymers **P1**−**P3** for the single-chain nanoparticle formation were prepared via post-polymerization modification of a random poly(styrene-*co*-chloromethylstyrene) copolymer (Scheme 2a). The copolymer was synthesized by NMP of styrene and 4-(chloromethyl)-styrene with 2,2,6,6-tetramethyl-1-(1-phenylethoxy)piperidine (compound **1**, Scheme 2a) as the initiator at 125 °C and subsequently characterized by ^{1}H NMR spectroscopy. The integral values for the proton resonances at 6.22−7.28 ppm (aromatic protons) and at 4.51 ppm (CH_2Cl) were utilized to determine the content of CMS in the copolymer, which was calculated to be 24% (see Figure S1). In a one-pot postpolymerization modification, the lateral chlorine atoms were substituted by a protected maleimide derivative (PG-Mal, compound **2**, Scheme 2a) and a tetrazole species (Tet, compound **3**, Scheme 2a) in various ratios. The incorporated ratio was calculated with the aid of the integral values for the resonances at 4.24, 5.01, and 5.26 ppm (resonances g, h, k, and p) in the proton NMR spectra of the functionalized polymers (refer to Figure S1). The specific functionality ratios, as well as the SEC characterization data of the linear, functional precursor polymers **P1**−**P3** are collated in Table S2.

A slight excess of Tet is necessary to reach the desired Tet/PG-Mal ratio and full conversion of the chlorine atoms (see Table S1). Contrary to common perception,[24] it was found that the electron-rich double bond of the PG-Mal moiety is still sufficiently reactive toward the nitrile imine and displays an increased performance in the intramolecular cross-linking reaction compared to the electron-deficient double bond of the deprotected maleimide. Initial attempts of the intramolecular cross-linking of the polymer to form SCNPs with the deprotected maleimide lead to poorer results, mostly to intermolecular cross-linking. Thus, the procedure was altered utilizing the protected maleimide moieties for the light-induced intramolecular cross-linking reactions, which significantly reduces the synthetic effort required for the linear precursor preparation (see Scheme 2a).

The intramolecular cross-linking of the linear precursors was carried out in highly diluted solutions ($c_{precursor}$ = 0.017 mg mL^{-1}) to afford the single-chain nanoparticles **SCNP1**−**SCNP3**. Due to the fluorescent nature of **SCNP2** and **SCNP3**, the kinetics of the intramolecular cross-linking process could be readily monitored by online fluorescence spectroscopy (see Figure S2). To achieve the best compromise between a good excitation of the photoreactive tetrazole and the fluorescence of the resulting pyrazoline derivative, an excitation wavelength of 315 nm was chosen for the irradiation of a diluted solution ($c_{precursor}$ = 0.017 mg mL^{-1}) of **P2** in THF. Inspection of Figure S2 shows that no further significant change in the fluorescence intensity occurs after 7 min, indicating that all accessible PG-Mal moieties have been consumed. Chemical evidence for the successful intramolecular cross-linking was obtained by ^{1}H NMR spectroscopy (refer to the Supporting Information for an exemplary spectrum, Figure S3). The formation of the pyrazoline cycloadduct leads to a decrease in intensity of the resonances corresponding to the PG-Mal moiety (resonances a and b, Figure S3) and a shift of the resonances corresponding to the aromatic protons of the Tet moiety to higher field (resonances c, d, e, Figure S3). Additional support for the intramolecular cross-linking is associated with the overall broadening of the resonances in the ^{1}H NMR spectrum. The broadening is caused by the loss of degrees of freedom during the cross-linking process.[25] Visualization of the SCNPs can be achieved by atomic force microscopy (AFM). Therefore, the SCNPs were drop-cast onto a freshly cleaved muscovite disc from diluted dichloromethane solution and vacuum-dried. During the casting process, dewetting phenomena and evaporative self-assembly may lead to aggregation of the SCNPs.[26,27] Thus, as discussed in earlier studies on the characterization of SCNPs by AFM, it should be noted that AFM can only act as a supporting analysis method and that SEC and DLS are the more reliable analytical tools.[14] Nevertheless, the particles (**SCNP2**) that were exemplary analyzed by AFM may indeed be SCNPs, as their average height (5.5 nm) is in the typical range for SCNPs (refer to

dx.doi.org/10.1021/mz500292e | *ACS Macro Lett.* 2014, 3, 574−579

Scheme 2. (a) Synthetic Route to the Functional Linear Precursors P1−P3 and for the Preparation of the (Pro)fluorescent Single-Chain Nanoparticles SCNP1−SCNP3;[a] (b) Synthetic Scheme for the Proof of Principle Reaction of the Profluorescent SCNP1 with Maleimide-Functional Microspheres (Mal-Microsphere); Residual Tetrazole Moieties of the Intramolecular Crosslinking are Utilized to Tether SCNP1 to the Mal-Microsphere

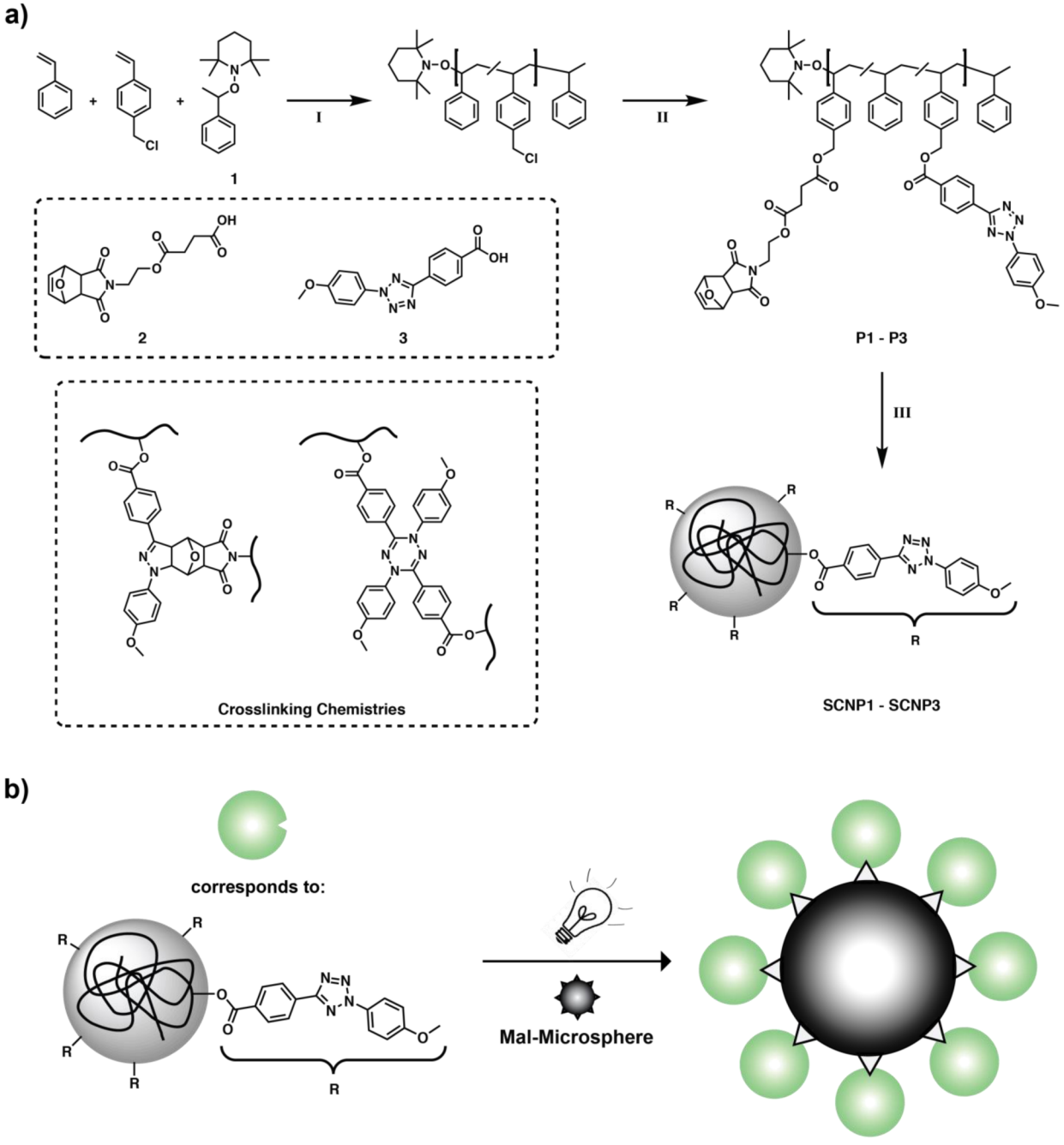

[a]Reagents and conditions: (I) bulk, 125 °C, 6 h; (II) **2**, **3**, Cs_2CO_3, DMF, 40 °C, 2 d; (III) $h\nu$, THF.

Figure S4 for the detailed particle analysis).[28] The AFM topography images depicted in Figure 1 display particles with a certain dispersity in size, which can be attributed to the already (limited) polydisperse nature of the linear precursors.

Due to tip-convolution effects, the diameter determined by AFM is beset with an error, yet under the assumption of spherical particles at least the obtained height can be interpreted as an approximate estimation for the size of the SCNPs. Although it appears compelling to compare the AFM and DLS results, it is not advisible to do so, since the SCNPs are in the solid state during AFM analysis and solvated during DLS measurements.

The coil-to-particle transition taking place during the intramolecular cross-linking process can be readily evidenced by size exclusion chromatography (SEC), since the SEC columns separate the analyte according to its hydrodynamic volume. Thus, the SCNP formation manifests itself in a shift of the SEC trace to longer retention times in comparison to the linear precursor (Figure 2, also Figure S5). With increasing tetrazole content (% Tet), the shift to longer retention times

dx.doi.org/10.1021/mz500292e | ACS Macro Lett. 2014, 3, 574−579

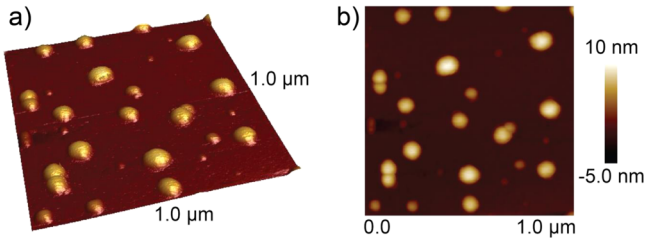

Figure 1. Three-dimensional (a) and two-dimensional (b) AFM topography images of **SCNP2** on freshly cleaved muscovite (scan size: 1 μm × 1 μm).

becomes more pronounced, which correlates with the assumption that the intramolecular cross-linking is mainly driven by the nitrile imine dimerization.

An estimation of the hydrodynamic diameter of the precursor polymers and the SCNPs can be performed by employing a power law, which was established by Fetters et al. (see Table 1).[29] Since the power law is based on empirical data, the obtained values should only serve as an approximation. Information on the actual hydrodynamic diameter of the SCNPs and the corresponding linear precursors was gathered by dynamic light scattering (DLS). The DLS results clearly support the trend that has already been observed in the SEC traces: The hydrodynamic diameter of the SCNP decreases with increasing tetrazole content (Figure 2, also Figure S5). It should be noted that the DLS traces of **SCNP1** and **SCNP2** exhibit a small second population at larger hydrodynamic diameters, which might be attributed to residual linear polymer or the product of intermolecular cross-links. The DLS and SEC results combined showcase that the size of the SCNPs can be fine-tuned by varying the ratio of functional groups along the backbone of the precursor polymer (see Table 1).

In addition to finely controlling the SCNPs' size, the current approach for SCNP formation allows for adjusting the fluorescence properties of the SCNPs by increasing the content of enes (% PG-Mal) among the cross-linking moieties with equal ease. With increasing PG-Mal content the probability of pyrazoline derivative formation during the intramolecular cross-linking also increases, leading to increased fluorescence intensity. Contrary to the pyrazoline derivative, the product of the nitrile imine dimerization does not exhibit fluorescence when excited at 415 nm. Exactly this trend is observed when examining the fluorescence properties of **SCNP1** to **SCNP3** (refer to Figure 3a,b). The excitation maximum (λ_{max}) of the pyrazoline derivative is close to 415 nm. When excited at λ_{max}, the maximum of the broad fluorescence emission band lies at 558 nm, therefore, in the biocompatible visible range. Thus, the particles are perfectly suitable for imaging of biological

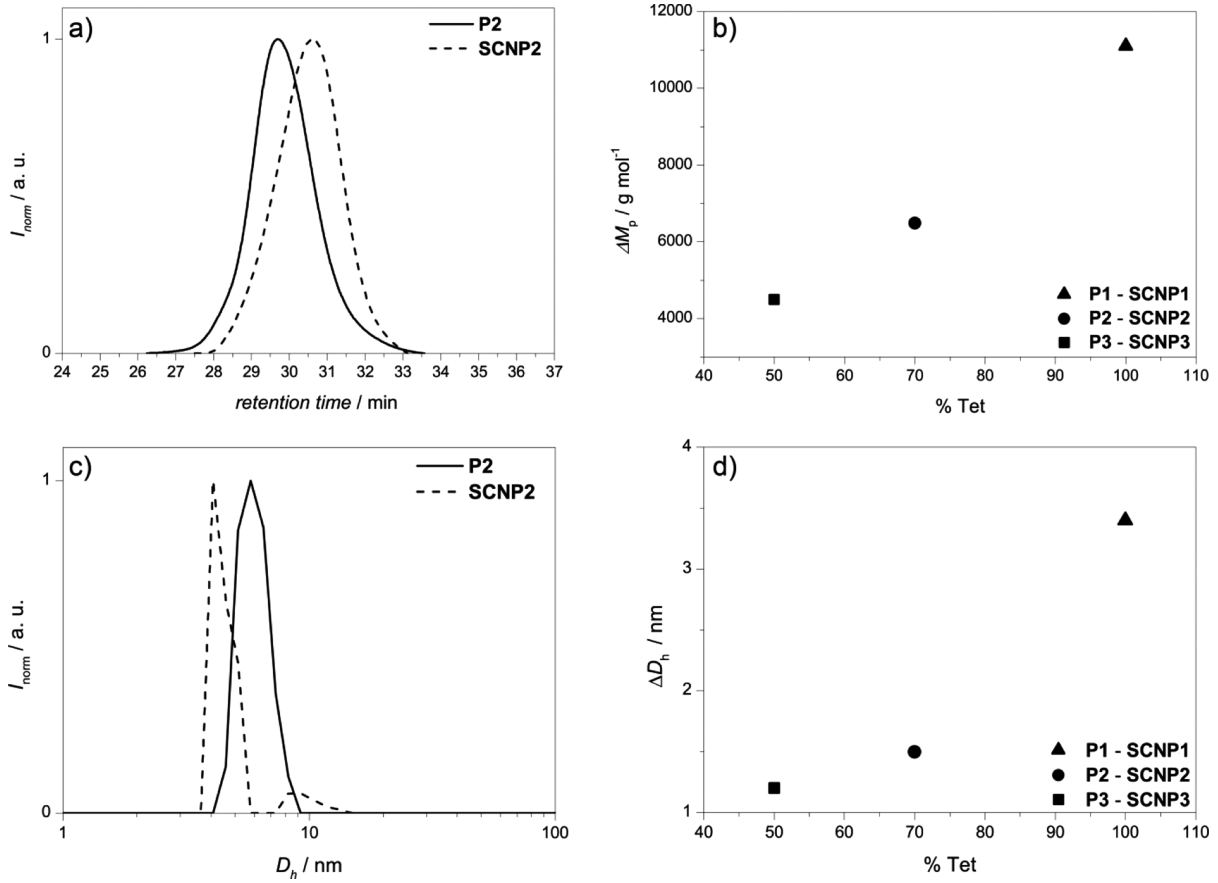

Figure 2. (a) Exemplary normalized SEC traces (THF, RI) of the linear precursors and single-chain nanoparticles (**P2**, **SCNP2**). (b) Change in peak molar mass (ΔM_p) after the single-chain collapse plotted against the tetrazole content (% Tet, relative to the number of initial CMS groups in the parent copolymer) of the linear precursor. (c) Exemplary number-weighted size distributions of the linear precursors and single-chain nanoparticles as determined by DLS (**P2**, **SCNP2**). (d) Change in mean hydrodynamic diameter (ΔD_h) after the single-chain collapse plotted vs the tetrazole content (% Tet, relative to the number of initial CMS groups in the parent copolymer) of the linear precursor (refer to the Supporting Information for the SEC and DLS results of the other samples).

dx.doi.org/10.1021/mz500292e | *ACS Macro Lett.* 2014, 3, 574−579

Table 1. SEC and DLS Results of the Functional Linear Precursor Polymers (P) and the Corresponding Single-Chain Nanoparticles (SCNP)

	SEC					DLS		
	M_p(P; g mol^{-1})	M_p(SCNP; g mol^{-1})	change (%)	$D_{h,SEC}$(P;[a] nm)	$D_{h,SEC}$(SCNP;[a] nm)	$D_{h,DLS}$(P; nm)	$D_{h,DLS}$(SCNP; nm)	collapse (%)
1	19500	8400	57	7.3	4.6	6.1	3.1	49
2	17800	11300	37	7.0	5.4	6.0	4.5	25
3	17000	12400	27	6.8	5.7	7.0	5.7	19

[a]As estimated by the power law established by Fetters et al.[29]

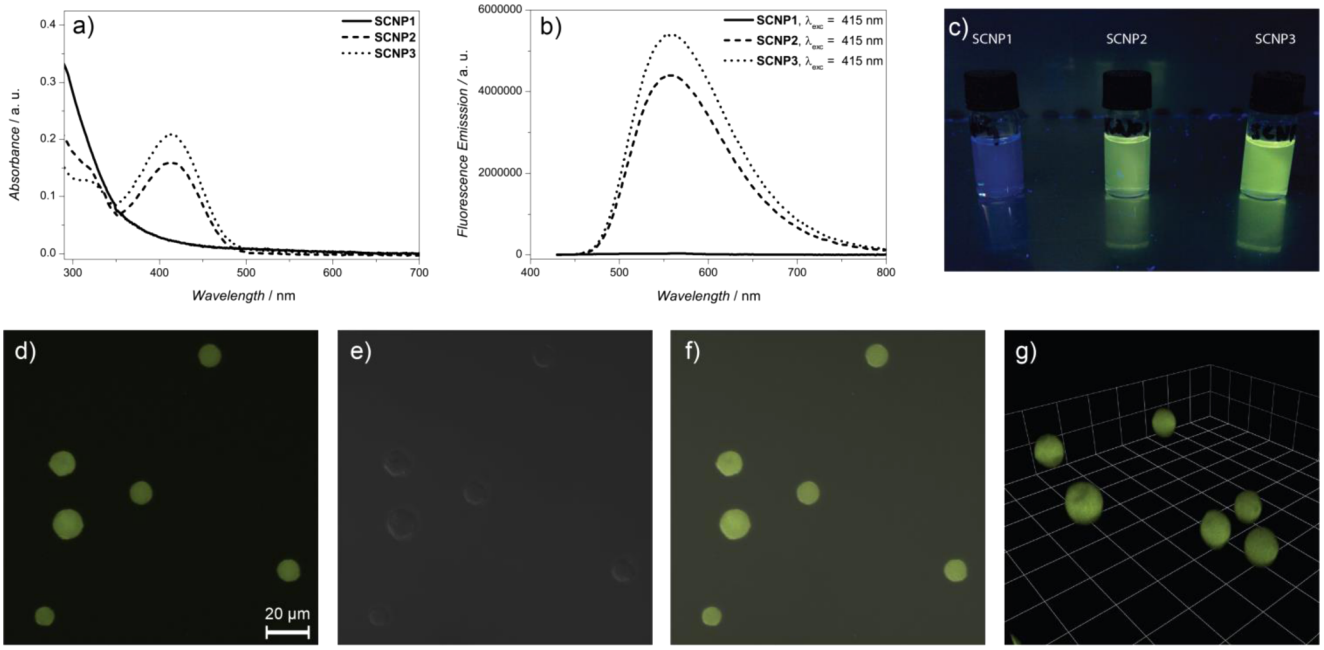

Figure 3. (a) UV/vis spectrum of **SCNP1−3** in DMF. (b) Fluorescence emission in DMF at an excitation wavelength of λ_{exc} = 415 nm. (c) Image of solutions of **SCNP1−SCNP3** in THF irradiated with a hand-held UV-lamp (λ = 366 nm). (d) Fluorescence microscopy image (142.86 μm × 142.86 μm) of the SCNP-functionalized microspheres (λ_{exc} = 405 nm, fluorescence detection from 530 to 600 nm). (e) Differential interference contrast (DIC) image of the same area. (f) Overlay of images (d) and (e). (g) Three-dimensional reconstruction of a confocal image stack showing the functionalized microspheres (1 unit = 14.3 μm).

processes since, for example, DNA and other large biomolecules are UV-sensitive. The profluorescent nature of **SCNP1** makes these single-chain nanoparticles the ideal candidate to showcase the functionalization ability of the presented SCNPs, since the success of the conjugation reaction leads to a fluorescent linkage, whereas the particles themselves do not fluoresce. In the current approach to functional SCNPs, residual tetrazole moieties after the single-chain cross-linking are utilized to attach the profluorescent **SCNP1** to maleimide-functional microspheres (Scheme 2b) to showcase their powerful ligation capability.

The conjugation of the tetrazole-functional single-chain nanoparticles to the maleimide-functional microspheres (Mal-Microsphere) was selected as a proof of principle, since the successful reaction can be readily monitored by fluorescence microscopy (Figure 3d−g). Inspection of Figure 3d−g demonstrates that all microspheres have been completely decorated with SCNPs. The employed maleimide-functional microspheres were synthesized from poly(glycidyl methacrylate) (PGMA) microspheres with a PGMA content of 80% and pore size of 1000 Å and have been thoroughly characterized in an earlier publication by our group.[30]

In summary, we present a powerful and facile to operate technology platform for the photoinduced preparation of functional, (pro)fluorescent single-chain nanoparticles (SCNPs) via phototriggered nitrile imine based intramolecular cross-linking of linear precursor polymers as imaging agents. The precursor polymers were synthesized by nitroxide mediated random copolymerization of styrene and 4-(chloromethyl)styrene followed by subsequent one-pot post-polymerization modification with a protected maleimide (PG-Mal) and tetrazole (Tet) moiety. We unambiguously demonstrate by SEC, DLS, UV/vis-, and fluorescence spectroscopy that by varying the ratio of functional moiety density, the size as well as the fluorescence properties of the SCNPs can be finely adjusted. In addition, we evidence in an exemplary reaction that the residual, surface expressed Tet moieties can be employed for further functionalization of the SCNPs. This, in combination with the fact that the SCNPs feature a broad fluorescence band (500−700 nm) in biocompatible excitation ranges (>400 nm), makes them ideal candidates for intracellular transport imaging applications for, for example, si-RNA or DNA delivery.

dx.doi.org/10.1021/mz500292e | ACS Macro Lett. 2014, 3, 574−579

■ ASSOCIATED CONTENT

Supporting Information

Experimental section, additional characterization data, and an illustration of the custom build photoreactor. This material is available free of charge via the Internet at http://pubs.acs.org.

■ AUTHOR INFORMATION

Corresponding Author

*Fax: (+49) 721 608 45740. E-mail: christopher.barner-kowollik@kit.edu.

Notes

The authors declare no competing financial interest.

■ ACKNOWLEDGMENTS

C.B.-K. acknowledges financial support from the Karlsruhe Institute of Technology (KIT) in the context of the Helmholtz BioInterfaces program, the German Research Council (DFG) and the Ministry of Science and Arts of the state of Baden-Württemberg. J.W. thanks Dipl. Phys. Benjamin Richter (Zoologisches Institut and Center for Functional Nanostructures, Karlsruhe Institute of Technology (KIT)) for the fluorescence microscopy images and Dipl.-Biol. Peter Krolla-Sidenstein (Institut für Funktionelle Grenzflächen (IFG), Karlsruhe Institute of Technology (KIT)) for the AFM analysis.

■ REFERENCES

(1) Altintas, O.; Barner-Kowollik, C. *Macromol. Rapid Commun.* **2012**, *33*, 958−971.
(2) Ouchi, M.; Badi, N.; Lutz, J.-F.; Sawamoto, M. *Nat. Chem.* **2011**, *3*, 917−924.
(3) Sanchez-Sanchez, A.; Pomposo, J. A. *Part. Part. Syst. Charact.* **2014**, *31*, 11−23.
(4) Altintas, O.; Lejeune, E.; Gerstel, P.; Barner-Kowollik, C. *Polym. Chem.* **2012**, *3*, 640−651.
(5) Willenbacher, J.; Altintas, O.; Roesky, P. W.; Barner-Kowollik, C. *Macromol. Rapid Commun.* **2013**, *35*, 45−51.
(6) Schmidt, B. V. K. J.; Fechler, N.; Falkenhagen, J.; Lutz, J.-F. *Nat. Chem.* **2011**, *3*, 234−238.
(7) Hosono, N.; Gillissen, M. A. J.; Li, Y.; Sheiko, S. S.; Palmans, A. R. A.; Meijer, E. W. *J. Am. Chem. Soc.* **2012**, *135*, 501−510.
(8) Appel, E. A.; Dyson, J.; del Barrio, J.; Walsh, Z.; Scherman, O. A. *Angew. Chem., Int. Ed.* **2012**, *51*, 4185−4189.
(9) Murray, B. S.; Fulton, D. A. *Macromolecules* **2011**, *44*, 7242−7252.
(10) Tuten, B. T.; Chao, D.; Lyon, C. K.; Berda, E. B. *Polym. Chem.* **2012**, *3*, 3068−3071.
(11) Oria, L.; Aguado, R.; Pomposo, J. A.; Colmenero, J. *Adv. Mater.* **2010**, *22*, 3038−3041.
(12) Chao, D.; Jia, X.; Tuten, B.; Wang, C.; Berda, E. B. *Chem. Commun.* **2013**, *49*, 4178−4180.
(13) Sanchez-Sanchez, A.; Akbari, S.; Etxeberria, A.; Arbe, A.; Gasser, U.; Moreno, A. J.; Colmenero, J.; Pomposo, J. A. *ACS Macro Lett.* **2013**, *2*, 491−495.
(14) Altintas, O.; Willenbacher, J.; Wuest, K. N. R.; Oehlenschlaeger, K. K.; Krolla-Sidenstein, P.; Gliemann, H.; Barner-Kowollik, C. *Macromolecules* **2013**, *46*, 8092−8101.
(15) He, J.; Tremblay, L.; Lacelle, S.; Zhao, Y. *Soft Matter* **2011**, *7*, 2380−2386.
(16) Frank, P. G.; Tuten, B. T.; Prasher, A.; Chao, D.; Berda, E. B. *Macromol. Rapid Commun.* **2014**, *35*, 249−253.
(17) Clovis, J. S.; Eckell, A.; Huisgen, R.; Sustmann, R. *Chem. Ber.* **1967**, *100*, 60−70.
(18) Song, W.; Wang, Y.; Qu, J.; Lin, Q. *J. Am. Chem. Soc.* **2008**, *130*, 9654−9655.
(19) Mueller, J. O.; Guimard, N. K.; Oehlenschlaeger, K. K.; Schmidt, F. G.; Barner-Kowollik, C. *Polym. Chem.* **2014**, *5*, 1447−1456.
(20) Blasco, E.; Piñol, M.; Oriol, L.; Schmidt, B. V. K. J.; Welle, A.; Trouillet, V.; Bruns, M.; Barner-Kowollik, C. *Adv. Funct. Mater.* **2013**, *23*, 4011−4019.
(21) de Hoog, H.-P. M.; Nallani, M.; Liedberg, B. *Polym. Chem.* **2012**, *3*, 302−306.
(22) Wang, J.; Zhang, W.; Song, W.; Wang, Y.; Yu, Z.; Li, J.; Wu, M.; Wang, L.; Zang, J.; Lin, Q. *J. Am. Chem. Soc.* **2010**, *132*, 14812−14818.
(23) Madden, M. M.; Rivera Vera, C. I.; Song, W.; Lin, Q. *Chem. Commun.* **2009**, 5588−5590.
(24) Dürr, C. J.; Lederhose, P.; Hlalele, L.; Abt, D.; Kaiser, A.; Brandau, S.; Barner-Kowollik, C. *Macromolecules* **2013**, *46*, 5915−5923.
(25) de Luzuriaga, A. R.; Ormategui, N.; Grande, H. J.; Odriozola, I.; Pomposo, J. A.; Loinaz, I. *Macromol. Rapid Commun.* **2008**, *29*, 1156−1160.
(26) Rabani, E.; Reichman, D. R.; Geissler, P. L.; Brus, L. E. *Nature* **2003**, *426*, 271−274.
(27) van Roekel, H. W. H.; Stals, P. J. M.; Gillissen, M. A. J.; Hilbers, P. A. J.; Markvoort, A. J.; de Greef, T. F. A. *Chem. Commun.* **2013**, *49*, 3122−3124.
(28) Berda, E. B.; Foster, E. J.; Meijer, E. W. *Macromolecules* **2010**, *43*, 1430−1437.
(29) Fetters, L. J.; Hadjichristidis, N.; Lindner, J. S.; Mays, J. W. *J. Phys. Chem. Ref. Data* **1994**, *23*, 619−640.
(30) Kaupp, M.; Tischer, T.; Hirschbiel, A. F.; Vogt, A. P.; Geckle, U.; Trouillet, V.; Hofe, T.; Stenzel, M. H.; Barner-Kowollik, C. *Macromolecules* **2013**, *46*, 6858−6872.